Plasticity in Aluminum Alloys at Various Length Scales

Wouters, Onne

Chapter 2

Experimental Techniques

The experimental work described in the subsequent chapters is aimed at understanding different aspects of the deformation process in metals and alloys. The deformation is studied at various length scales, requiring multiple microscopic techniques. This chapter describes various techniques used and explains in a concise way how the deformation is applied to the testing materials.

2.1 Microscopy

Since its advent in the early 1930s, the electron microscope has become an invaluable tool in materials research. By utilizing the very short wavelengths of electrons, information about the microstructure of materials was obtained, that would have remained hidden if only light microscopy had been used. In our work two different types of electron microscopes are used. After a short description of the Scanning Electron Microscope (SEM), considerable more details are provided about the operation of a Transmission Electron Microscope (TEM) and in particular the image formation process which is less obvious than that of an SEM. Further details of electron microscopy can be found in the following textbooks [1-4].

2.1.1 Scanning Electron Microscopy

When an electron beam of sufficient energy impinges onto a material, a number of different interaction processes take place, which can for a large portion be used in the SEM. Normal imaging in an SEM is done by scanning a highly focused electron beam, with an energy usually between 3 and 30 keV, over the surface of the material of interest while collecting the secondary electrons. These are electrons that are knocked out from the material by the primary electrons. Since their mean free path is

usually very small (~10 Å), they can be used to form high resolution images of the specimen surface.
Primary electrons that are backscattered from the top surface of the material are interesting because the backscattering cross section depends strongly on the atomic number (*Z*) of the atom the electron collides with. Scanning the surface and collecting the backscattered electrons thus yields a map of the surface with high *Z*-contrast.
When a primary electron penetrates the inner electron shells and enough energy is transferred to one of the core electrons, it can be ejected. The ionized atom will relax to the ground state by filling the vacant position with one of the outer shell electrons. This process is accompanied by either the emission of an X-ray or an Auger electron, the energies of which are *Z*-specific. Collection of X-ray spectra in an SEM is quite common, making a chemical analysis of the surface possible. Auger detection is less common, although dedicated Auger microscopes exist.

2.1.2 Transmission Electron Microscopy

Figure 2.1 gives a schematic overview of a TEM. An electron beam is generated by

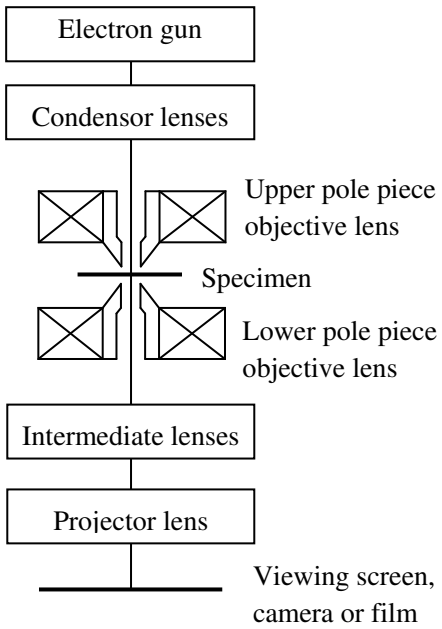

Figure 2.1 *Schematic impression of a transmission electron microscope.*

the electron gun, which is either a thermionic or a field emission source. In a thermionic source electrons are emitted from a heated tungsten filament or from a LaB_6 crystal. In a field emission gun (FEG), which is a cold source, the electrons are extracted from a very sharp tip using a high electric field. The electron beam produced by a FEG is more monochromatic, has a higher spatial coherency and a much higher brightness than the beam produced by a thermionic source. The latter however is more stable and since the FEG produces a very narrow beam, it is more difficult to illuminate large areas. In all sources the emitted electrons are accelerated to energies typically between 100 and 400 keV. The condenser lens assembly is used to create a parallel beam of electrons, which will pass the specimen, that has been thinned enough to make it transparent to the electron beam. It is this transmitted beam that is transferred through the microscope column and finally forms an image that can be recorded.

Although the transmission of the electron beam depends on the mass of the atoms in the specimen foil and therefore so-called mass-thickness contrast can be seen in the image, the principal strength of conventional TEM lies in the possibility to create diffraction contrast. When the specimen is crystalline, electrons will be diffracted by crystal planes. With a TEM it is possible to switch easily between the imaging mode and the diffraction mode as is illustrated in Figure 2.2. The left picture shows the ray paths of the electron beam after passage through the specimen in imaging mode. The electrons are focused by the objective lens assembly. As can be seen by following the rays in the picture, electrons that have been diffracted by the same angle are focused at the same position in the back-focal plane of the objective lens. In the column, this is the first occurrence of the diffraction pattern. The image is reconstructed in the image plane of the objective lens. This image is then projected by the intermediate lenses and finally by the projector lens onto either a fluorescent viewing screen, an electron sensitive film or a CCD camera. To make the diffraction pattern visible, the microscope is switched to diffraction mode (Fig. 2.2b). The intermediate lens is weakened, making the back focal plane of the objective lens coincide with the object plane of the projector lens.

Apertures can be inserted in the back focal plane of the objective lens to select specific regions of the diffraction pattern. The image is formed with only those electrons that have been diffracted by specific crystal planes. This is the basis of diffraction contrast imaging. Most commonly a two-beam technique is used, for which the specimen is tilted in such a way that only one crystal plane is in a diffraction condition. In the diffraction pattern only two beams are now visible: the direct beam of non diffracted electron and one diffraction spot. With the objective aperture one of the two beams is selected and an image is formed. If the direct beam

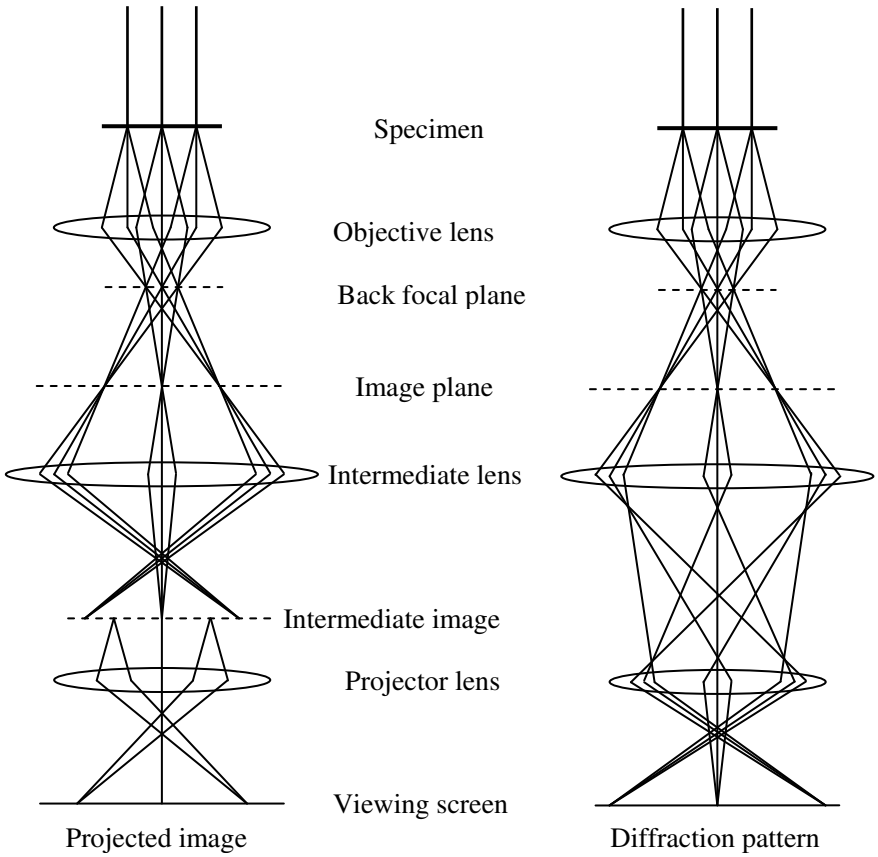

Figure 2.2 *Ray paths for the two main modes of operation in the TEM. Left: imaging mode. Right: diffraction mode.*

is used the image is called a bright field (BF) image. If the diffracted beam is used, a dark field (DF) image is formed. When dynamic effects are ignored, the origin of the contrast is straightforward. The darker regions in the BF image and the brighter regions in the DF image correspond to those regions where more electrons were diffracted i.e. where the planes are more in diffraction condition. Hence it becomes possible to create contrast between different phases, grains, defects etc.

TEM research consists for a substantial part of interpreting the contrast that is observed in the recorded micrographs. Small differences in contrast under special diffraction conditions make it possible to distinguish between different kinds of defects. To observe these differences, a good understanding of the origins of the contrast is necessary and therefore the following sections will describe in detail the nature of diffraction by (non perfect) crystals.

Diffraction from a crystal

The incoming electrons are scattered by the atoms in the material as a result of Coulomb interaction with the negatively charged electron cloud and the positively charged nucleus. The scattered electrons will only interfere constructively when certain diffraction conditions are met. One way to describe these conditions is by applying Bragg's law, which states that the difference in path length traveled by two beams deflected from parallel planes has to be an integer number of wavelengths:

$$2d \sin \theta_B = n\lambda \qquad (2.1)$$

where d is the interplanar spacing, θ_B is the so-called Bragg angle between the incoming beam and the diffracting plane, n is an integer and λ is the wavelength of the incoming electrons.
Another way to describe the diffraction condition is by switching to reciprocal space. Diffraction occurs when:

$$\boldsymbol{k}_g = \boldsymbol{k}_0 + \boldsymbol{g} \qquad (2.2)$$

where $\boldsymbol{k_0}$ is the wave vector of the incoming electron beam, $\boldsymbol{k_g}$ is the wave vector of the diffracted beam and $\boldsymbol{g}$ is a reciprocal lattice vector. A very elegant and in electron microscopy very useful representation of this, is the Ewald sphere construction [5]. In reciprocal space the $\boldsymbol{k_0}$ vector is drawn with its endpoint coinciding with the origin of the reciprocal lattice and its starting point as the center of a sphere with radius 1/λ (Fig. 2.3).

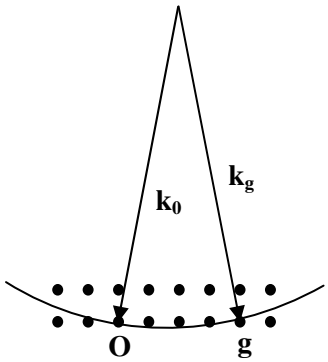

Figure 2.3 *Part of the Ewald sphere in the reciprocal lattice [1].*

Diffraction now occurs if the Ewald sphere intersects another reciprocal lattice point, since only then the difference between the diffracted and incoming wave vector will be equal to a reciprocal lattice vector.

The amplitude of the diffracted beam can be written as:

$$A(\boldsymbol{g}) = F_g \sum_L \exp(2\pi i \boldsymbol{s} \cdot \boldsymbol{A}_L) \tag{2.3}$$

where F_g is the so-called structure factor and is defined as:

$$F_g = \sum_j f_j \exp(2\pi i \boldsymbol{g} \cdot \boldsymbol{\rho}_j) \tag{2.4}$$

Since $\boldsymbol{\rho}_j$ is the position of atom j in the unit cell and f_j is the atomic scattering factor of the same atom, the structure factor defines the amplitude scattered by one unit cell in the direction defined by $\boldsymbol{g}$. This structure factor is important because it turns out that for several $\boldsymbol{g}$-vectors the summation (2.4) will for a specific crystal structure be equal to zero. For an fcc lattice for example, the {001} and {011} reflections, will not occur. They are referred to as forbidden reflections. In equation (2.3) the summation is made over all unit cells *L*. $\boldsymbol{A_L}$ are the real space lattice positions and $\boldsymbol{s}$ is called the deviation parameter, which is defined as the vector pointing from the reciprocal lattice point *G* to the place on the Ewald sphere, where the diffracted wave vector $\boldsymbol{k}$ ends ($\boldsymbol{k}=\boldsymbol{k_0}+\boldsymbol{g}+\boldsymbol{s}$). For diffraction in a bulk specimen, with many unit cells in all directions, this would mean that $A(\boldsymbol{g})$ only takes a value unequal to zero when $\boldsymbol{s}$ is exactly zero. In the TEM however, the specimen is very thin and therefore the number of unit cells in the direction normal to the foil is not very large. As a result diffraction spots will be seen even if the diffraction condition (2.2) is not exactly met. In the Ewald sphere construction this can be expressed by replacing the spots in reciprocal space by little rods (so-called relrods) perpendicular to the foil plane. Considering also that due to the small wavelength of the electrons, the Ewald sphere is very large with respect to the reciprocal lattice spacing, it is now clear why in reality often a whole row of reflections (a systematic row) is visible in a diffraction pattern.

Diffraction and imaging of defects

Since the scattering angle of the diffraction events is very small (~1 mrad), it is justified to assume that they all take place in a narrow column parallel to the incoming electron beam. The diffraction inside the column is independent of what happens in neighboring columns. In a perfect crystal all the columns will diffract is a similar way and no contrast will be seen in the final image. If however, the crystal is not perfect, local variations in $\boldsymbol{s}=s(x,y,z)$ will be present. The amplitude of a diffracted wave for the column at (x,y) is:

$$A_g(x,y) = F_g \int_0^t \mathrm{e}^{2\pi i s(x,y,z)z} dz \tag{2.5}$$

Using this column approximation a set of coupled differential equations can be derived for the case of only one strong diffracting beam (s is much larger or smaller than zero for all other $\boldsymbol{g}$ vectors). These Howie-Whelan equations [6] describe the change in amplitude of the direct beam φ_0 and the amplitude of the diffracted beam φ_g considering also dynamical effects arising from multiple diffraction. A derivation can be found in any textbook on TEM (e.g. [1-4]). They are:

$$\frac{d\phi_g}{dz} = \frac{\pi i}{\xi_g}\phi_0 e^{-2\pi i s z} + \frac{\pi i}{\xi_0}\phi_g \tag{2.6}$$

and

$$\frac{d\phi_0}{dz} = \frac{\pi i}{\xi_0}\phi_0 + \frac{\pi i}{\xi_g}\phi_g e^{2\pi i s z} \tag{2.7}$$

where ξ_0 and ξ_g are called the extinction coefficients for the direct and diffracted beam. From these equations it follows that the amplitude of the diffracted beam continuously increases and decreases when the beam moves through the specimen. These equations are valid for a perfect crystal but can be modified easily to account for defects by introducing the displacement field $\boldsymbol{R}$, which defines the displacement at any point with respect to the normal lattice. It can be shown that the Howie-Whelan equations can be written as:

$$\frac{d\phi_g}{dz} = \frac{\pi i}{\xi_0}\phi_g + \frac{\pi i}{\xi_g}\phi_0 e^{-2\pi i(sz+\boldsymbol{g}\cdot\boldsymbol{R})} \tag{2.8}$$

and

$$\frac{d\phi_0}{dz} = \frac{\pi i}{\xi_0}\phi_0 + \frac{\pi i}{\xi_g}\phi_g e^{2\pi i(sz+\boldsymbol{g}\cdot\boldsymbol{R})} \tag{2.9}$$

Therefore, when the displacement field of a specific defect is known, the Howie-Whelan equations can be used to deduce the contrast that will arise in a micrograph formed by making a BF or a DF image using $\boldsymbol{g}$.

Contrast from a dislocation

Dislocations are line defects inside a crystal, which contribute to the plasticity of materials. Therefore a study of the deformation behavior of a crystalline material is

in essence a study of the nucleation and propagation of dislocations. Chapter 3 concentrates entirely on dislocations and their role in the mechanical properties of metals. For now it is only important that a dislocation can be characterized by a vector, the so-called Burgers vector ***b***. Figure 2.4 is a schematic picture of an edge dislocation, showing the Burgers vector. In a BF or DF image contrast arises because, as can be seen in the figure, the planes around the dislocation are bent. Since in the through foil direction the Bragg condition is relaxed, i.e. the reciprocal lattice points are actually relrods, there will be contrast even if the component of ***s*** along the columns is unequal to zero. The value of *s* changes due to the bent planes, and therefore the contrast changes and the dislocations will be seen as a line. If the specimen is tilted such that in the parts of the lattice far away from the dislocation *s* slightly deviates from zero, the presence of the dislocation will bend the planes on one side more into perfect Bragg orientation and the planes on the other side farther away. This effect gives rise to the typical bright-dark line pairs often seen in BF or DF images.

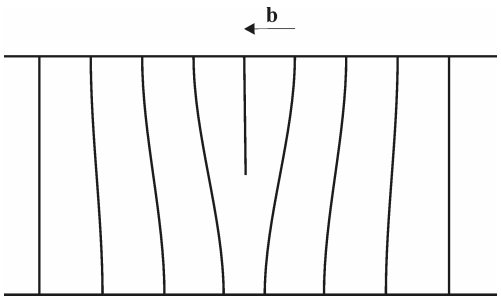

Figure 2.4 *Schematic drawing of an edge dislocation with Burgers vector **b**. The planes around the dislocation are bent. This curvature can be used to attain a diffraction condition for which only the dislocation region is in Bragg condition.*

The displacement fields around different types of dislocations are known. For a screw type dislocation (explained in chapter 3) ***R*** is everywhere exactly parallel to the Burgers vector ***b.*** For an edge type dislocation this is only true to a first approximation. To determine the contrast caused by dislocations, the ***g·R*** product in the Howie-Whelan equations can be replaced by a term proportional to ***g·b***. This implies that dislocations give no contrast when:

$$\boldsymbol{g} \cdot \boldsymbol{b} = 0 \qquad (2.10)$$

This is called the invisibility criterion and it is very useful in determining the Burgers vector of a dislocation. By tilting the specimen such that different ***g*** vectors

are used to image a dislocation and by finding two reflections $\mathbf{g}_1$ and $\mathbf{g}_2$ for which the invisibility criterion holds, the Burgers vector may be determined using:

$$(\boldsymbol{g}_1 \times \boldsymbol{g}_2) \| \boldsymbol{b} \tag{2.11}$$

Weak beam imaging

When calculating the contrast produced by a dislocation, it can be shown that the width of the line contrast becomes smaller when s increases. This fact is used in what is called weak beam dark field imaging. By making s very large it becomes possible to create well-localized, sharp images of dislocations. A trade-off has to be made since the amplitude of the diffracted beam for such a high value of s is very low and long exposure times are necessary whereas drift may become a problem. The results however are dark pictures with bright sharp lines, indicating the positions of the dislocations. This technique is especially useful when dislocations close to each other have to be imaged or when small dislocation loops have to be identified.
In practice the specimen is tilted in such a way that a $\boldsymbol{g}$ vector nearly obeys the Bragg condition, after which the beam is tilted until this $\boldsymbol{g}$ is on the optical axis. As can be seen in Figure 2.5, the Ewald sphere now passes almost through the $3\boldsymbol{g}$ reflection that becomes excited. The image however is made with the $\boldsymbol{g}$ reflection, which has become very weak due to the large value of s.

High Resolution Transmission Electron Microscopy

According to the Huygens principle, the wave function $\psi(\boldsymbol{r})$ at the exit face of the specimen can be considered as a planar source of spherical waves. The amplitude of the diffracted wave $\psi(\boldsymbol{g})$, with $\boldsymbol{g}$ a reciprocal lattice vector or spatial frequency, is given by the Fourier transform of $\psi(\boldsymbol{r})$.

$$\psi(\boldsymbol{g}) = F\psi(\boldsymbol{r}) \tag{2.12}$$

where F is the Fourier transform operator. The intensity distribution in the back focal plane of the objective lens (i.e. the diffraction pattern) is equal to $|\psi(\boldsymbol{g})|^2$. In an ideal microscope the imaging system will, by an inverse Fourier transform, subsequently transform $\psi(\boldsymbol{g})$ back into the final image wave function $\Phi(\boldsymbol{r})$.

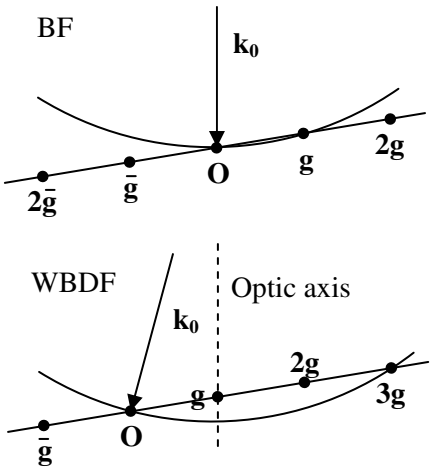

Figure 2.5 *For weak-beam dark field imaging first a bright field two beam condition is set up (top). Next, the beam is tilted such that the initially bright* **g** *reflection is moved onto the optic axis. The Ewald sphere almost exactly crosses the 3***g** *reflection, which therefore will be excited (bottom). The image is made using the now very weak* **g** *reflection [1].*

However, a perfect microscope does not exist. In fact electromagnetic lenses are far worse than optical lenses. Especially the outermost beams are heavily influenced by spherical and chromatic aberrations and have to be blocked using an aperture. The spherical aberrations and the defocus in the remaining beam will however still cause a considerable phase shift $\chi(\boldsymbol{g})$ with respect to the central beam. The wave function in the image plane can be written as:

$$\Phi(\boldsymbol{r}) = F^{-1}T(\boldsymbol{g})F\psi(\boldsymbol{r}) \tag{2.13}$$

where

$$T(\boldsymbol{g}) = A(\boldsymbol{g})\exp[-i\chi(\boldsymbol{g})] \tag{2.14}$$

is called the contrast transfer function. $A(\boldsymbol{g})$ describes the aperture. The function is unity for $\boldsymbol{g}$'s allowed to pass the aperture and zero for $\boldsymbol{g}$'s blocked by the aperture. The phase shift $\chi(\boldsymbol{g})$ is given by:

$$\chi(\boldsymbol{g}) = \tfrac{1}{2}\pi C_s \lambda^3 g^4 + \pi\varepsilon\lambda g^2 \tag{2.15}$$

where C_s is the spherical aberration coefficient, ε the defocus, λ the electron wavelength and g is the magnitude of $\boldsymbol{g}$.

Figure 2.6 shows the typical shape of a transfer function. At low g, the function has a stretched plateau with values close to -1, which corresponds to a phase shift of π/2. For higher g, i.e. for higher spatial frequencies or smaller image details, the function starts to oscillate around zero and the resulting contrast is far less intuitive. The ideal defocus value is that which extends the plateau maximal. This is called Scherzer defocus. Now imagine we try to image a weak phase object, i.e. the phase part of the wave function $\varphi(\boldsymbol{r}) \ll 1$. The object wave function can be approximated by:

$$\psi(\boldsymbol{r}) \approx 1 + i\varphi(\boldsymbol{r}) \tag{2.16}$$

The constant term 1 contributes to the central beam and the term $i\varphi$ to the diffracted beams. If the phase is shifted by the transfer through the microscope by π/2, the amplitudes of the diffracted beams are multiplied by exp(iπ/2) and $i\varphi(\boldsymbol{r})$ becomes $-\varphi(\boldsymbol{r})$. The amplitude of the image wave function becomes:

$$\Phi(\boldsymbol{r}) = 1 - \varphi(\boldsymbol{r}) \tag{2.17}$$

and, since φ is small, its intensity is given by:

$$\left|\Phi(\boldsymbol{r})\right|^2 \approx 1 - 2\varphi(\boldsymbol{r}) \tag{2.18}$$

Due to the π/2 phase shift the final image has become a direct representation of the weak phase object. The same principle was used by F. Zernike in his phase contrast light microscope, which earned him the 1953 Nobel Prize in physics.
A thin foil specimen will act as a phase object, in which the phase is proportional to the electrostatic potential projected along the beam direction. If the specimen therefore is tilted such that columns of atoms are parallel to the beam, the image will show atoms as dark spots and empty space as light areas. The point resolution of the

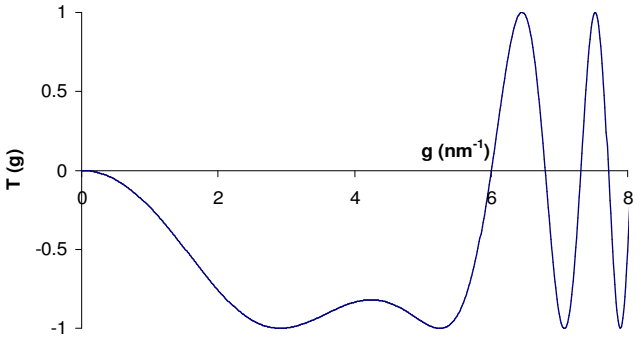

Figure 2.6 *Contrast transfer function for a TEM with Cs is 0.97 mm, λ=1.6 pm and ε= 47 nm.*

microscope is defined as the finest detail that can be directly interpreted in terms of the structure. At Scherzer defocus, the point resolution corresponds to the *g* of the first zero in the contrast transfer function. The information limit of the microscope is much better, but in order to get useful information out of the area beyond the point resolution, image simulations and a good knowledge of the contrast transfer function are necessary.
Table 2.1 summarizes some of the important characteristics for the two types of microscopes used in this thesis.

Table 2.1 *Main characteristics of the two transmission electron microscopes used for this thesis.*

	JEOL 4000EX/II	JEOL 2010F
Emission	LaB_6 crystal	Field emission gun
Operating voltage (kV)	400	200
Spherical aberration coefficient (mm)	0.97	1.0
Information limit (nm)	0.14	0.11
Point resolution (nm)	0.165	0.23
Optimum defocus (nm)	47	58

2.1.3 Orientation Imaging Microscopy

Orientation Imaging Microscopy (OIM) is a rather recent technique, in which an SEM is used to collect information about the orientation of surface grains in the specimen. It uses the principle of Electron Backscatter Diffraction (EBSD). When the focused electron beam in the SEM collides with the specimen, electrons originating from a reasonable small volume are scattered in all directions. These scattered electrons can be diffracted from the lattice planes following the rules described above. Since the electrons hit the diffracting plane from all directions, those electrons exactly fulfilling the Bragg condition lie on the surface of two so-called Kossel cones, one cone formed by the electrons diffracted from the top of the plane and one cone formed by those electrons diffracted from the bottom of the plane.
The diffracted electrons are collected by placing a fluorescent screen close to the specimen. The intercepted cones will appear on the screen as two nearly straight lines forming a band. These Kikuchi bands will appear for all the planes provided the structure factor (Eq. 2.4) is not equal to zero. A typical EBSD pattern from an aluminum specimen is shown in Figure 2.7. To maximize the yield during an OIM

scan, the specimen is tilted 70° with respect to the incident electron beam. The beam is scanned over the surface and at every point, an EBSD pattern is collected. Software codes are subsequently used to index the patterns. Finally an orientation map of the specimen surface is obtained. In this research OIM is used to determine grain size values, texture information and deformation profiles within grains.

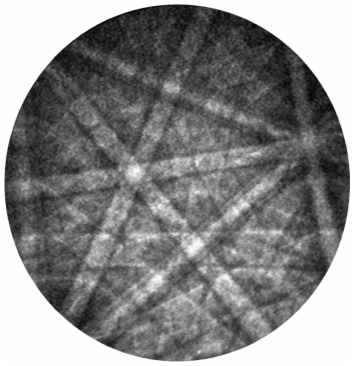

Figure 2.7 *Typical electron back-scattered diffraction pattern for an fcc lattice.*

2.1.4 Confocal Microscopy

The most common way to obtain topographic height maps over micrometer scales is to use some kind of profilometer, where a needle like object is scanned over the surface and its vertical deviation is a measure of the topography of the specimen surface. A few disadvantages of this technique, mainly its poor lateral resolution due to the finite stylus radius, and the damage it can cause to the specimen, are not present when a confocal microscope is used. The principle of the confocal microscope is rather simple and dates back to 1957, when it was presented by Minsky [7,8]. Light emitted from a laser or white light source passes an illumination pinhole, a beam splitter and an objective lens, which converges the beam onto the sample. The setup is chosen such that only when the beam is focused on the surface the reflected light, converged again by the objective lens and redirected by the beam splitter, passes the confocal or detector pinhole after which it is collected by a detector. When the surface is slightly out of focus, less reflected light will pass the pinhole and reach the detector.

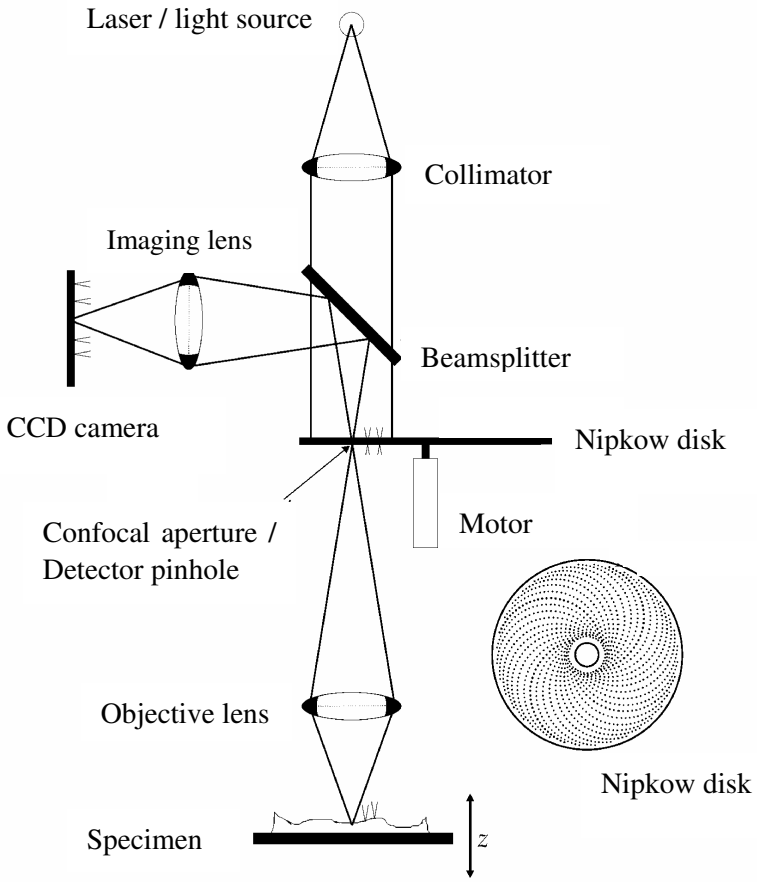

Figure 2.8 *Schematic setup of a scanning confocal microscope. Only the light reflected off the surface that is focused by the objective lens on the detector pinhole is transmitted to the camera. A Nipkow disk is used to scan a regular pattern on the specimen surface [9].*

In the modern confocal microscope, the principle of Minsky is adapted slightly. A picture of such an instrument is seen in Figure 2.8 [9]. A collimator lens creates a parallel beam, which passes first through a beam splitter and then through a rotating Nipkow disk, which acts as a multiple point source scanning the surface. The light from a single hole in the disk is focused onto the surface by the objective lens. When the specimen is exactly in focus, the reflected light will be refocused onto the same hole in the Nipkow disk, after which the beam splitter and an imaging lens will form an image on the detector. The Nipkow disk, which is in fact both the illumination and detector pinhole, makes it possible to get topographic information from a fixed grid of points with a single capture of the CCD detector. The objective lens can now

be moved very accurately using a piezo-device, bringing different parts of the specimen in focus.
The intensity of the beam at the detector can be described with a simple formula:

$$I(z) = I_0 \left(\frac{\sin(kz(1-\cos\alpha))}{kz(1-\cos\alpha)} \right)^2 \qquad (2.19)$$

where α is the aperture angle of the objective lens, k is the wavenumber of the radiation, z is the defocusing coordinate and I_0 is the intensity at the detector when the sample is exactly in focus ($z=0$). The variation of I with z is given in Figure 2.9.

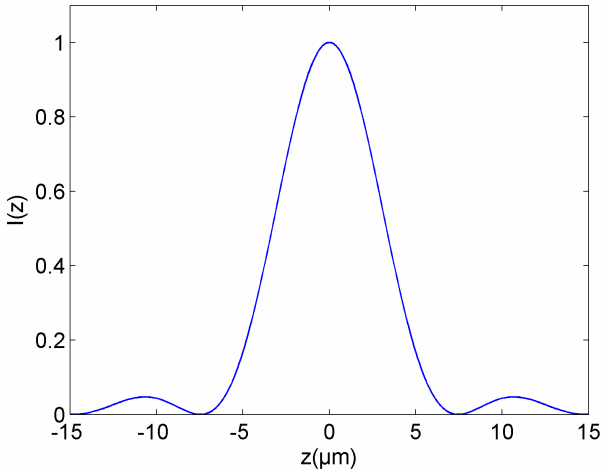

Figure 2.9 *The intensity of the beam at the detector as a function of the specimen height z calculated for a 20x objective lens and a wavelength of λ=400 nm.*

Since we have moved every point in the grid completely through focus, the problem of finding the height at a point x,y is reduced to calculating the center of gravity of the peak in equation 2.19 i.e:

$$h(x,y) = \frac{\sum_{z_k \in FWHM} I(x,y,z_k) \cdot z_k}{\sum_{z_k \in FWHM} I(x,y,z_k)} \qquad (2.20)$$

where the summation is only taken over those z_k values within the peak's full width at half maximum to reduce noise effects occurring in the profile's tail.

2.1.5 Atomic Force Microscopy

Although the confocal microscope is very well suited to make topographic maps of larger surfaces, its lateral resolution is limited to several hundreds of nanometers. When height information on a smaller scale is required, an atomic force microscope (AFM) can be used. An AFM is a very small probing tip at the free end of a cantilever with a low spring constant. The tip is moved into close proximity with the specimen surface. Due to the forces acting on the tip that are exerted by the specimen surface atoms, the cantilever will be deflected. This deflection is detected and can be used as a measure of the distance between tip and surface. However, the relationship between the surface-tip distance and the force on the tip is not an easy one. Several forces play a role. The tip is close enough to the surface to feel the chemical forces, which can be attractive or repulsive, it will feel the Van der Waals forces and on some surfaces a layer of water or hydrocarbons will be present which can exert capillary forces on the tip. Therefore most AFMs do not work in constant-height mode but rather in constant-force mode. They are equipped with a feedback system that will adjust the height of the tip using piezo-devices such that the deflection of the cantilever i.e. the force on the tip remains constant.
To minimize surface damage while maintaining fast scanning times, in this work the so-called *tapping mode* AFM is used. A piezoelectric actuator drives the cantilever into an oscillatory motion with a frequency close to its natural frequency. Since in tapping mode the cantilever only touches the surface in the bottom of its swing, the forces exerted on the surface are low and no shear stresses will arise. The interaction forces with surface atoms will change the amplitude of the oscillation and its phase with respect to the driving signal. Again, topographic information is acquired by

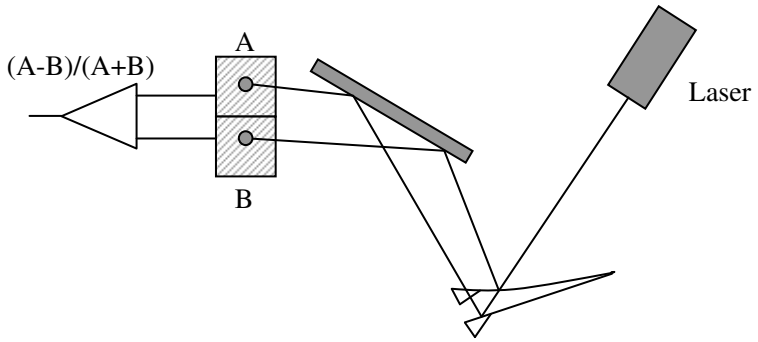

Figure 2.10 *The deflection of the tip in an AFM is detected using a laser beam focused on the end of the cantilever. The differential signal of the two detectors A and B is a measure of this deflection and is used as the feedback signal in the AFM.*

adjusting the height of the tip to compensate for these changes.
The movement of the tip is detected by an optical lever technique (Fig. 2.10). A laser beam is focused on the end of the cantilever. The light reflected by the cantilever is collected by two or four closely packed photodiodes. A change in deflection of the cantilever will result in a change of the differential output signal of the detector (A-B)/(A+B). In tapping mode this signal will be sinusoidal and its rms-value serves as the AFM feedback signal.
For the work described in this thesis, a Digital Instruments Dimension 3100 SPM is used, which allows scans up to 100x100 µm with vertical range of 6 µm. The height resolution is mainly limited by thermal noise. If sufficient measures are taken to reduce vibrational noise, the resolution may be as good as 0.05 nm.

2.2 Experiments

2.2.1 Tensile deformation

In the subsequent chapters in this thesis the effects of tensile deformation on metallic, mainly aluminum, specimens is studied. To deform the material a special tensile stage is used. This small stage (Fig. 2.11) has especially been built to be mounted inside a scanning electron microscope and is later modified to be also fitted under an optical, a confocal and an atomic force microscope, enabling a diverse number of in-situ straining experiments.
Figure 2.12 shows a typical tensile specimen. This particular one has a v-shaped

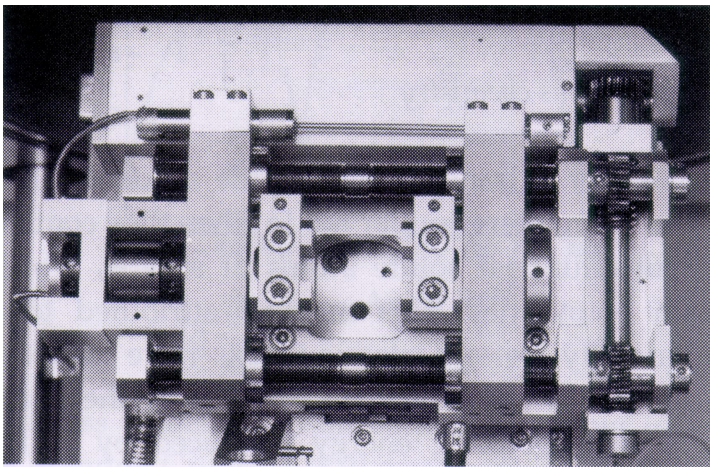

Figure 2.11 *Tensile stage used for most of the experiments.*

notch but also samples without a notch or with a rounded notch are used. The thickness of the specimens is limited by the load cell of the tensile stage, which can only handle loads below 5000N. The crosshead speed of the stage can be varied from 0.2 up to 25 µm/s and the possibility exists to heat up the specimen during deformation. For this purpose, a ceramic heating element is mounted in the stage just below the specimen. This heating element is strong enough to heat the specimen up to a temperature of 1000 °C. All heating experiments in chapter 6 are performed with the tensile stage inside the vacuum of the SEM. This prolongs the lifetime of the element and minimizes the influence of corrosion on deformation and fracture.

Figure 2.12 *Typical shape of a tensile specimen. The notches are added only when large stress concentrations are desirable.*

2.2.2 Sample preparation

For most experiments described in this thesis, good sample preparation is essential. Most techniques, e.g. SEM, EBSD, confocal microscopy, AFM and nano-indentation, require very flat surfaces for optimal imaging or accuracy. Polishing aluminum samples can be difficult since most of the alloys used are very soft. As a consequence polishing diamonds may get stuck in the aluminum or the material gets smeared out rather than polished away. The latter problems leaves an optically smooth surface but will not reveal any EBSD patterns since too much of the crystallinity in the surface layer has been lost. Basically, three different approaches have been used, depending on the problems encountered and the experimental techniques intended to be used. First, a strictly mechanical polishing approach has been used, consisting of grinding down the specimens with SiC-paper with grain sizes decreasing till a grade 1200 paper. Next, the ground specimens are polished with 6 µm, 3 µm and 1 µm diamond pastes. The final step is a polishing treatment with a SiO_2 suspensions. This technique works fine for SEM imaging.
Unfortunately, this mechanical approach will leave some sort of deformed surface layer, which will deteriorate the EBSD patterns and may influence hardness measurements using the nano-indenter. Also the surface morphology changes, which are to be detected by AFM and confocal microscopy, can be influenced by a deformed surface layer. This layer can be removed by chemical techniques. The best

results are obtained using electrochemical polishing. The electrolyte used for this research is a 5% perchloric acid solution in methanol at a temperature of -30 °C. The specimen is used as anode and the stainless steel container as cathode. The applied voltage is 20V.

For creating EBSD patterns, chemical polishing yields the best results. After mechanically polishing as described above, the specimens are submerged for no longer than 20 seconds in a solution consisting of 80% water, 20% nitric acid and 0.5% HF to which 9 grams of CrO_3 powder are added. This treatment will not actually polish the surface but the HF will remove all oxides such as SiO_2 residues. Furthermore the top layer which contains all the deformation will be etched away. Roughening of the surface will not influence the EBSD maps, but makes this technique unsuitable for AFM, confocal microscopy and SEM).

TEM specimens are all prepared similarly. Laser-cut discs with a diameter of 3 mm are ground to a thickness of 150 µm and are subsequently electrochemically polished inside a jet-polisher, which shoots electrolyte from both sides onto the disc. The electrolyte, temperature and voltage are similar as above. With an optical system, the jets are turned off at the moment a hole has been shot in the centre of the specimen. The material close to this hole is now thin enough to be observed inside the TEM.

References

1. D.B. Williams and C.B. Carter, *Transmission Electron Microscopy*, Plenum Press, 1996
2. S. Amelinckx, D. van Dijck, J. van Landuyt and G. van Tendeloo, *Handbook of Microscopy, Methods I*, VCH, 1997
3. B. Fultz and J.M. Howe, *Transmission Electron Microscopy and Diffractometry of Materials*, Springer Verlag, 2001
4. J.W. Edington, *Monographs in Practical Electron Microscopy in Materials Science*, The Philips Technical Library, 1976
5. D.W.J. Cruickshank, H.J. Juretschke and N. Kato Eds. *P.P. Ewald and his Dynamical Theory of X-ray Diffraction*, Oxford University Press, 1992
6. A. Howie and M.J. Whelan, *Proc. Roy. Soc.* A263, 217, 1961
7. M. Minsky, Microscopy Apparatus, USA patent 3013467, 1961
8. M. Minsky, *Scanning* 10, 128-38, 1988
9. H.J. Jordan, M. Wegner and H. Tiziani, *Meas. Sci. Technol.* 9, 1142-51, 1998